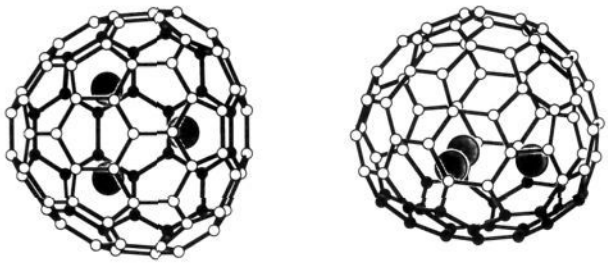

a b

1

this ab initio treatment, the a''_2 orbital is the cluster SOMO (singly occupied MO) and the general correspondence with better theory is encouraging. The energy level diagram we calculate for the C_{82} fragment is similar to results obtained by Manolopoulos using the simple Hückel method.[13]

Many of the endohedral fullerene complexes have been interpreted as species with encapsulated ions, $M_x^{n+}@C_m^{n-}$. As a rough approximation $Sc_3@C_{82}$ can be formulated as $Sc_3^{2+}@C_{82}^{2-}$, but this neglects some important mixing between unoccupied C_{82}^{2-} orbitals and the Sc_3^{2+} fragment. Figure 1 shows the percentage of fullerene character in the highest occupied and lowest unoccupied levels for C_{82}^{2-}; the mixing is evident. In contrast, Mulliken population of the occupied C_{82}^{2-} orbitals show that they generally retain greater than 90% fullerene character. A key result of our calculations is that the most bonding orbital for the Sc_3 fragment interacts strongly with several low-lying C_{82} orbitals and is destabilized. Consequently, this orbital is pushed much higher in energy and is unoccupied in the $Sc_3@C_{82}$ molecule. $Co_3(CO)_9S$, $FeCo_2(CO)_9S$, and $Ni_3(CO)_2(C_5H_5)_3$ are particular examples involving trinuclear metal clusters similar to the Sc_3 fragment in $Sc_3@C_{82}$ and are instances in which EPR studies confirm the symmetry and detailed nature of the highest occupied molecular orbital.[18,19] As in this instance, the 4s cluster orbitals are strongly destabilized by interaction with occupied ligand-based orbitals and are pushed well into the unoccupied manifold.[19] C_{82}^{2-} and other fullerenes are unique ligands that may stabilize otherwise unisolable clusters, but it is clear that fullerene cages do not comprise "inert matrices" for the endohedral species which they envelop.

The interaction diagram for $Sc_3@C_{82}$ in Figure 1 shows how the fullerene cage induces significant shuffling in the ordering of the Sc_3 cluster MOs. Four orbitals with varying degrees of Sc_3 character are occupied in the $Sc_3@C_{82}$ molecule, and each of these orbitals is significantly modified from the form that the occupied orbitals take in the free cluster. The SOMO of the naked Sc_3 fragment is of a''_2 symmetry, but it is destabilized after interaction with the cage. The SOMO in the $Sc_3@C_{82}$ molecule is of a_1 symmetry and is largely derived from the 2nd lowest valence orbital of the naked Sc_3 after mixing with the LUMO and other orbitals of the C_{82}^{2-} fragment. Several of the lowest unoccupied molecular orbitals of the C_{82} fragment mix significantly into the four highest occupied orbitals of the endohedral cluster. Accounting of the 337 electrons of $Sc_3@C_{82}$ places a single unpaired electron in the nondegenerate orbital, which is consistent with the EPR results for this molecule.

We should acknowledge that our placement of the Sc_3 cluster within the C_{82} cage is arbitrary with respect to the vertical positioning of the cluster (see **1a**). Calculations with the cluster placed at different 3-fold sites were performed and yield similar results with respect to the overall qualitative interaction between the Sc_3 fragment and the surrounding carbon framework, but the resulting HOMO–LUMO gaps are smaller. The measured shift in the *g*-value (1.9985) indicates that the cluster's unpaired electron resides in a nondegenerate orbital (a_1 or a_2) that is spaced reasonably far in energy from orbitals which can contribute to the ground state via spin–orbit coupling (a_2 or a_1, respectively). We obtain the best agreement with the EPR results with the calculations discussed above. More convincing structural evidence awaits the isolation of $Sc_3@C_{82}$ in greater quantities.

Acknowledgment. We gratefully acknowledge the National Science Foundation for its support through a Presidential Young Investigator Award (Grant DMR-8858151).

(18) Longuet-Higgins, H. C.; Stone, A. J. *Mol. Phys.* **1962**, *5*, 417.
(19) Strouse, C. E.; Dahl, L. F. *Discuss. Faraday Soc.* **1969**, *47*, 93.

Pulsed-Field Gradient-Enhanced Three-Dimensional NMR Experiment for Correlating $^{13}C\alpha/\beta$, $^{13}C'$, and $^{1}H\alpha$ Chemical Shifts in Uniformly ^{13}C-Labeled Proteins Dissolved in H_2O

Lewis E. Kay

Protein Engineering Network Centres of Excellence and Departments of Medical Genetics, Biochemistry, and Chemistry, Medical Sciences Building University of Toronto, Toronto, Ontario, Canada, M5S 1A8

Received November 24, 1992

The development of multinuclear, multidimensional NMR spectroscopy has greatly increased the size limitations of proteins whose structures can be solved by NMR methods.[1-7] The first class of experiments developed consists of those which detect the NH chemical shift during acquisition and hence must be recorded on samples dissolved in H_2O. The second class of experiments, including the HCACO and the HCA(CO)N experiments among others, detects the Hα resonances during acquisition, and spectra are obtained on samples dissolved in D_2O.[1-2] The development of pulsed field gradient technology offers the attractive possibility of recording the latter class of experiments in H_2O, as well, by using these gradients to suppress the undesired water resonance. This has the significant advantage in that all of the spectra necessary for obtaining backbone assignments can be recorded on a single sample, thus eliminating ambiguities with comparing chemical shifts from samples which were prepared under slightly different conditions and which can show significant isotope shifts of the ^{15}N and carbonyl (C′) resonances.[1] In this communication, a pulsed-field gradient experiment is presented for correlating Cβ/α, C′, and Hα chemical shifts. Gradients are used to suppress the intense water signal which would otherwise obscure many of the cross-peaks.

Figure 1 illustrates the pulse sequence that is employed to provide the Cβ/α, C′, Hα correlations. The path of magnetization transfer can be described concisely as

$$H\beta/\alpha \xrightarrow{J_{CH}} C\beta/\alpha(t_1) \xrightarrow{J_{C\alpha C\beta}} C\alpha \xrightarrow{J_{C\alpha C'}} C'(t_2) \xrightarrow{J_{C\alpha C'}} C\alpha \xrightarrow{J_{CH}} H\alpha(t_3)$$

where the active couplings involved in each magnetization-transfer step are indicated above each arrow. The gradient pulses were positioned in the sequence in order to minimize the water signal and aid in the elimination of artifacts.[8-10] The first gradient pulse,

(1) Ikura, M.; Kay, L. E.; Bax, A. *Biochemistry* **1990**, *29*, 4659.
(2) Kay, L. E.; Ikura, M.; Tschudin, R.; Bax, A. *J. Magn. Reson.* **1990**, *89*, 496.
(3) Clubb, R. T.; Thanabal, V.; Wagner, G. *J. Biomol. NMR* **1992**, *2*, 203.
(4) Grezesiek, S.; Bax, A. *J. Magn. Reson.* **1992**, *96*, 432.
(5) Farmer, B. T.; Venters, R. A.; Spicer, L. D.; Wittekind, M. G.; *Muller*, L. *J. Biomol. NMR* **1992**, *2*, 195.
(6) Palmer, A. G.; Fairbrother, W. J.; Cavanaugh, J.; Wright, P. E.; Rance, M. *J. Biomol. NMR* **1992**, *2*, 103.
(7) Grezesiek, S.; Bax, A. *J. Am. Chem. Soc.* **1992**, *114*, 6291.
(8) Hurd, R. E.; John, B. K. *J. Magn. Reson.* **1991**, *91*, 648.
(9) Von Kienlin, M.; Moonen, C. T. W.; Van Der Toorn, A.; Van Zijl, P. C. M. *J. Magn. Reson.* **1991**, *93*, 423.
(10) Bax, A.; Pochapsky, S. *J. Magn. Reson.* **1992**, *99*, 638.
(11) Bax, A.; Freeman, R. *J. Am. Chem. Soc.* **1981**, *44*, 542.
(12) Sørensen, O. W. *J. Magn. Reson.* **1990**, *90*, 405.
(13) McCoy, M.; Mueller, L. *J. Am. Chem. Soc.* **1992**, *114*, 2108.
(14) Shaka, A. J.; Barker, P. B.; Freeman, R. *J. Magn. Reson.* **1985**, *64*, 547.

0002-7863/93/1515-2055$04.00/0

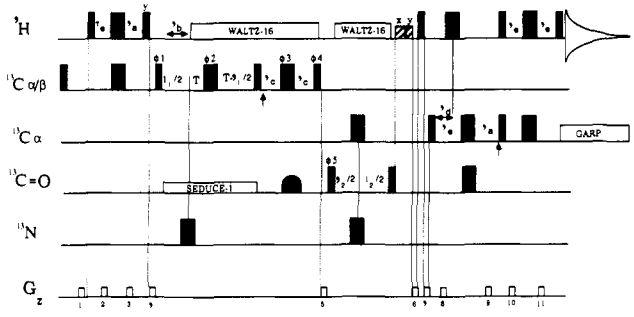

Figure 1. Pulse sequence for correlating $^{13}C\alpha/\beta$, C′, and Hα chemical shifts. The $^{13}C\alpha/\beta$ chemical shifts are recorded in a constant time manner.[11,12] All narrow pulses have a flip angle of 90°, while wider pulses have an angle of 180°. Pulses for which the phases are not indicated are applied along the x axis. The $^{13}C\alpha/\beta$ and $^{13}C\alpha$ pulses are applied at 43 and 54 ppm, respectively. The field strengths employed are as follows: $^{13}C\alpha/\beta$ 180$\phi 2$ = 16.3 kHz; other $^{13}C\alpha/\beta$ 180° (90°) pulses = 9.8 kHz (4.4 kHz); $^{13}C\alpha$ 180° (90°) pulses = 9.0 kHz (4.0 kHz); C′ rectangular pulses = 4.0 kHz; SEDUCE-1[13] decoupling = 625 Hz, GARP[14] decoupling = 2.2 kHz, WALTZ-16[15] decoupling = 6.0 kHz. The shaped C′ 180° (250 μs) pulse is applied immediately after the Cα/β 180$\phi 3$ pulse with a shape profile given by a 180° element in the SEDUCE-1[13] decoupling scheme. The second C′ 180° pulse is applied immediately prior to the Cα 180° pulse in the τ_e interval. The C′ pulses are applied as phase-modulated pulses.[16,17] To aid in the suppression of the water signal, 10-kHz purge pulses of duration 6 (along x) and 3.5 ms (along y) are applied after the t_2 evolution period. The arrows in the sequence indicate the position of application of the C′ pulses to compensate for the Bloch–Siegert[18-20] effects of the C′ 180° pulses indicated in the sequence. The delays used are τ_a = 1.8 ms, τ_b = 2.1 ms, τ_c = 4.3 ms, τ_d = 1.8 ms, τ_e = 2.7 ms, and T = 3.6 ms. The value of τ_c was chosen to maximize the intensities of the $^{13}C\beta$, C′, Hα cross-peaks. The duration and strengths of the gradients are 1 = (0.5 ms, 4G/cm), 2 = 3 = (1 ms, 15 G/cm), 4 = (2ms, 25 G/cm), 5 = (5 ms, 27 G/cm), 6 = (7ms, 30 G/cm), 7 = (4.0ms, 30 G/cm), 8 = 9 = (1.3ms, 20 G/cm), 10 = 11 = (1.3ms, 14 G/cm). All gradients are applied along the z axis and are rectangular. A delay of at least 50 μs is inserted between a gradient pulse and the subsequent application of an rf pulse. The phase cycle is $\phi 1 = x$; $\phi 2 = x, y, -x, -y$; $\phi 3 = \phi 4 = 4(x), 4(-x)$, $\phi 5 = 8(x), 8(-x)$; receiver = $2(x,-x), 2(-x,x), 2(-x,x), 2(x,-x)$. Quadrature in t_1 and t_2 is obtained by States-TPPI[21] of $\phi 1$ and $\phi 5$.

applied after the 90° ^{13}C pulse at the beginning of the sequence, ensures that magnetization giving rise to signal originates on ^1H and not ^{13}C. Gradient pulse pairs 2 and 3 and 10 and 11 ensure that only ^1H single quantum magnetization present during both τ_a periods contributes to observed magnetization.[10] (In nongradient applications, the first $^{13}C\alpha/\beta$ 180° pulse would normally be phase cycled $\pm x$[7]). Following the 90_y ^1H pulse, the desired magnetization is along the z axis, while the water magnetization is in the transverse plane. A gradient pulse is applied at this time to dephase the transverse water magnetization. A gradient pulse applied between the C$\alpha/\beta(\phi 4)$ and C′($\phi 5$) pulses suppresses any transverse magnetization which could give rise to spectral artifacts while leaving the desired magnetization of the form $S_zC'_z$(S = $^{13}C\alpha$) untouched. Immediately following the second 90° $^{13}C'$ pulse after the t_2 period, proton x and y purge pulses are applied to suppress the water signal and are followed by the application of a gradient pulse. Residual water magnetization along the z axis is subsequently brought into the transverse plane by a 90° ^1H pulse and eliminated through the action of an additional gradient pulse. The gradient pulses applied during the τ_e periods suppress artifacts created by imperfections in the 180° $^{13}C\alpha$ refocusing pulse and, in addition, eliminate any transverse ^1H (solvent) magnetization

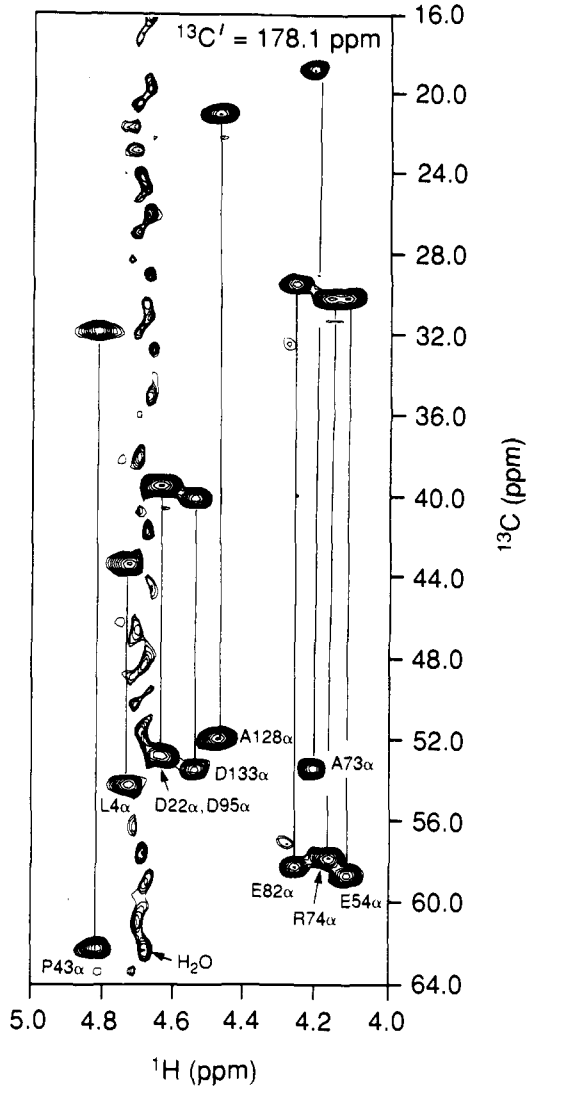

Figure 2. $F_1(^{13}C\alpha/\beta) - F_3(^1H\alpha)$ slice at a C′ shift of 178.1 ppm. The data set was recorded as a 52 × 64 × 512 complex matrix. Acquisition times of 7.1, 42.7, and 64.0 ms were recorded in (t_1,t_2,t_3) with a relaxation delay of 0.8 s, giving rise to a total measuring time of 53 h. After data processing, including linear prediction in the t_1 time domain, the size of the absorptive part of the matrix was 256x128x1024. No data massaging to remove the residual water was applied.

created by an imperfect ^1H 180° pulse. Immediately prior to the final ^1H 90° pulse, the magnetization of interest is along the x axis; the small amount of water magnetization which has recovered due to longitudinal relaxation during $2\tau_e$ and acted upon by the ^1H pulses during the INEPT back-transfer is parallel to the y axis. The final 90_x ^1H pulse rotates this magnetization back to the z axis immediately prior to detection, while leaving the desired signal unaffected.

The phase cycling used in this experiment can be reduced by the insertion of gradient pulse pairs on opposite sides of the $^{13}C\alpha/\beta$ pulses $\phi 2$ and $\phi 3$ in Figure 1. In this case, the phase cycling of $\phi 3$ can be eliminated and that of $\phi 2$ reduced to (x,y). If axial peaks in t_1 can be tolerated, the latter phase cycle can also be eliminated. However, since the application of gradient pulses during decoupling interferes with the decoupling and can lead to a substantial decrease in the signal, it is important that the gradient pulses be applied when the decoupling is off. Since 16 transients/FID were accumulated for this application, no attempt to reduce the number of phase cycling steps below 16 was made.

The experiment was recorded on a 1.5 mM uniformly ^{15}N, ^{13}C-labeled sample of *Xenopus laevis* calmodulin complexed with 4 equiv of Ca^{2+} in 90% H_2O, 10% D_2O, 37 °C. The experiment was performed on a Varian UNITY-500 spectrometer equipped

(15) Shaka, A. J.; Keeler, J.; Frenkiel, T.; Freeman, R. *J. Magn. Reson.* **1983**, *52*, 335.
(16) Boyd, J.; Scoffe, N. *J. Magn. Reson.* **1989**, *85*, 406.
(17) Patt, S. L. *J. Magn. Reson.* **1992**, *96*, 94.
(18) Vuister, G. W.; Bax, A. *J. Magn. Reson.* **1992**, *98*, 428.
(19) McCoy, M. A.; Mueller, L. *J. Magn. Reson.* **1992**, *99*, 19.
(20) McCoy, M. A.; Mueller, L. *J. Magn. Reson.* **1992**, *98*, 674.
(21) Marion, D.; Ikura, M.; Tschudin, R.; Bax, A. *J. Magn. Reson.* **1989**, *85*, 393.

with a pulsed-field gradient accessory and a triple resonance probe with an actively shielded z gradient. No water presaturation was used. Figure 2 illustrates an $F_1(^{13}C\alpha/\beta) - F_3(^1H\alpha)$ slice at a C′ shift of 178.1 ppm. The slight amount of residual water does not pose a problem for the observation of correlations to Hα protons that resonate at or very near the water line.

In summary, a pulsed field gradient experiment is presented which correlates $^{13}C\alpha/\beta$, $^{13}C'$, and $^1H\alpha$ chemical shifts with high sensitivity. The field gradient approach described here is equally applicable to other experiments such as the HCACO and HCA(CO)N and should greatly facilitate recording of all of the triple resonance backbone experiments in H_2O.

Acknowledgment. The author thanks Dr. Mitsu Ikura, Ontario Cancer Institue, Toronto, Canada for kindly providing the sample of ^{15}N, ^{13}C-labeled calmodulin used in this study and Drs. Luciano Mueller, Mike Wittekind, and Sandy Farmer, Bristol-Myers Squibb, New Jersey for valuable discussions. This research was supported, in part, by a grant to L.E.K. from the Natural Sciences & Engineering Research Council of Canada.

Preparation, Catalytic Reactivity, and X-ray Crystal Structure of the First Group 4 Alkyl/Alkene Complexes. The First Structural Models of the Key Ziegler–Natta Catalytic Intermediate

Michael D. Spencer, Paige M. Morse, Scott R. Wilson, and Gregory S. Girolami*

School of Chemical Sciences
The University of Illinois at Urbana-Champaign
505 South Mathews Avenue, Urbana, Illinois 61801

Received August 20, 1992

We herein describe the preparation and reactivity of the first group 4 complexes that contain both an alkyl ligand and a coordinated alkene; these complexes are the first group 4 molecular analogues of the key alkyl/alkene intermediate[1,2] that just precedes the insertion step in the mechanism of the Ziegler–Natta polymerization of alkenes. Interestingly, some of these complexes are active catalysts for the dimerization of alkenes.

Alkylation of $HfCl_4$ with 6 equiv of ethyllithium in diethyl ether at −78 °C, followed by warming to room temperature and addition of *N,N,N′,N′*-tetramethylethylenediamine (tmed), gives colorless crystals of the remarkable species $[Li(tmed)]_2[Hf(C_2H_4)Et_4]$ (**1**), which is formally an ethylene complex of Hf[1,3,4] The ^{13}C NMR

$$HfCl_4 + 6LiEt + 2tmed \rightarrow [Li(tmed)]_2[Hf(C_2H_4)Et_4] + 4LiCl + C_2H_6$$

spectrum of **1** in C_7D_8 at 20 °C contains a triplet at δ 30.5 due to the ethylene ligand; the $^1J_{CH}$ coupling constant of 119 Hz is unprecedentedly low for an ethylene ligand. In comparison, $^1J_{CH}$ coupling constants for all other transition-metal ethylene complexes are 144 Hz or larger and are typically 150–160 Hz.[5-8]

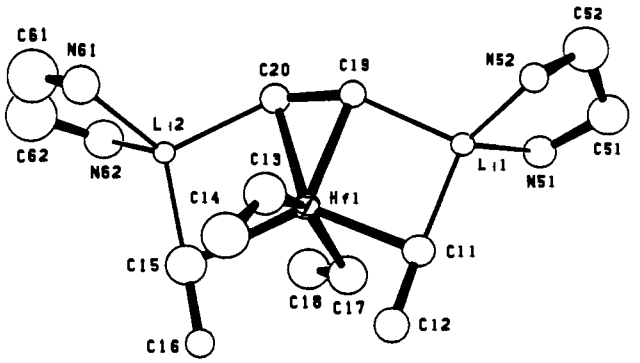

Figure 1. Molecular structure of $[Li(tmed)]_2[Hf(C_2H_4)Et_4]$. Thermal ellipsoids are represented by the 35% probability surfaces; the methyl groups of the tmed ligands have been omitted for clarity. Important bond distances (Å) and angles (deg) for molecule 1: Hf(1)–C(19) 2.26(4), Hf(1)–C(20) 2.31(4), Hf(1)–C(11) 2.39(5), Hf(1)–C(15) 2.45(4), Hf(1)–C(13) 2.38(4), Hf(1)–C(17) 2.43(6), C(19)–C(20) 1.49(6), Li(1)–C(19) 2.40(9), Li(2)–C(20) 2.37(9), Li(1)–C(11) 2.05(8), Li(2)–C(15) 2.04(9), Hf(1)–C(13)–C(14) 109(3), Hf(1)–C(17)–C(18) 110(4), Hf(1)–C(11)–C(12) 101(3), Hf(1)–C(15)–C(16) 105(3), C(13)–Hf(1)–C(17) 149(2), C(11)–Hf(1)–C(15) 132(1), C(11)–Hf(1)–C(19) 94(2), C(15)–Hf(1)–C(20) 97(2).

The formation of the $[Hf(C_2H_4)Et_4^{2-}]$ dianion presumably proceeds via the hexaethylhafnate complex $[HfEt_6^{2-}]$, which would be analogous with the known[9] hexamethylhafnate species $[HfMe_6^{2-}]$. However, $[HfEt_6^{2-}]$ is evidently unstable and spontaneously loses 1 equiv ethane. The gases evolved upon treating $HfCl_4$ with 2,2,2-trideuterioethyllithium ($LiCH_2CD_3$) were analyzed by GC/MS and were found to consist almost exclusively of ethane-d_4. This result clearly shows that the principal pathway for formation of the $[Hf(C_2H_4)Et_4^{2-}]$ dianion is β-elimination.

The X-ray crystal structure[10] of $[Li(tmed)]_2[Hf(C_2H_4)Et_4]$ reveals that the complex can best be considered as a square-based pyramid with the ethylene ligand occupying the axial position and the four ethyl groups occupying the basal sites (Figure 1). The $[Li(tmed)^+]$ cations bridge between the ethylene ligand[11] and two

(1) (a) Cossee, P. *Tetrahedron Lett.* **1960**, 12–16. (b) Cossee, P. *Tetrahedron Lett.* **1960**, 17–21. (c) Cossee, P. *J. Catal.* **1964**, *3*, 80–88. (d) Arlman, E. J.; Cossee, P. *J. Catal.* **1964**, *3*, 99–104. (e) Cossee, P. *Recl. Trav. Chim. Pays-Bas* **1966**, *85*, 1151–1160. (f) Rodriguez, L. A. M.; van Looy, H. M. *J. Polym. Sci. Part A-1* **1966**, *4*, 1971–1992, and references therein.

(2) Boor, J. *Ziegler–Natta Catalysts and Polymerizations*; Academic Press: New York, 1979; Chapter 13.

(3) Anal. Calcd for **1**: C, 46.4; H, 9.94; N, 9.84; Li, 2.24; Hf, 31.4. Found: C, 46.3 H, 9.76; N, 9.83; Li, 2.77; Hf, 30.6. ^1H NMR (C_7D_8, 20 °C): δ 0.31 (s, Hf-C_2H_4); 0.05 (q, J_{HH} = 7.5, Hf-CH_2Me); 2.06 (t, J_{HH} = 7.5, Hf-CH_2Me); 2.00 (s, NMe_2); 1.70 (s, NCH_2). ^{13}C NMR (C_7D_8, 20 °C): δ 31.0 (t, J_{CH} = 119, Hf-C_2H_4); 41.9 (t, J_{CH} = 106, Hf-CH_2Me); 13.8 (q, J_{CH} = 121, Hf-CH_2Me); 45.9 (q, J_{CH} = 132, NMe_2); 56.5 (t, J_{CH} = 136, NCH_2). $^{13}C\{^1H\}$ NMR (CPMAS, −50 °C): δ 31.7 (s, Hf-C_2H_4); 46.7 (s, Hf-CH_2Me); 14.8 (s, Hf-CH_2Me); 48.0 (s, NMe_2); 57.7 (s, NCH_2).

(4) Few hafnium alkene complexes are known. See: (a) Takahashi, T.; Tamura, M.; Saburi, M.; Uchida, Y.; Negishi, E. *J. Chem. Soc., Chem. Commun.* **1989**, 852–853. (b) Buchwald, S. L.; Kreutzer, K. A.; Fisher, R. A. *J. Am. Chem. Soc.* **1990**, *112*, 4600–4601.

(5) Mann, B. E.; Taylor, B. F. *^{13}C NMR Data for Organometallic Compounds*; Academic Press: New York, 1981; Table 2.10.

(6) (a) Fellmann, J. D.; Schrock, R. R.; Rupprecht, G. A. *J. Am. Chem. Soc.* **1981**, *103*, 5752–5758. (b) Fellmann, J. D.; Schrock, R. R.; Traficante, D. D. *Organometallics* **1982**, *1*, 481–484.

(7) Cohen, S. A.; Auburn, P. R.; Bercaw, J. E. *J. Am. Chem. Soc.* **1983**, *105*, 1136–1143.

(8) For discussions of $^1J_{CC}$ coupling constants, C–C bond distances, and the degree of π-back-bonding to alkene ligands, see: Tolman, C. A.; English, A. D.; Manzer, L. E. *Inorg. Chem.* **1975**, *14*, 2353–2356. Chisholm, M. H.; Huffman, J. C.; Hampden-Smith, M. J. *J. Am. Chem. Soc.* **1989**, *111*, 5284–5299. Brookhart, M.; Volpe, A. F.; Lincoln, D. M.; Horvath, I. T.; Millar, J. M. *J. Am. Chem. Soc.* **1990**, *112*, 5634–5636. Bender, B. R.; Norton, J. R.; Miller, M. M.; Anderson, O. P.; Rappe, A. K. *Organometallics* **1992**, *11*, 3427–3434.

(9) Morse, P. M.; Girolami, G. S. *J. Am. Chem. Soc.* **1989**, *111*, 4114–4116.

(10) Crystal data for $C_{22}H_{56}N_4Li_2Hf$ (T = 198 K): orthorhombic, space group *Pbca*, a = 21.513(9) Å, b = 17.443(4) Å, c = 32.100(7) Å, V = 12046(11) Å^3, Z = 16, R_F = 0.077, and R_{wF} = 0.078 for 244 variables and 2216 unique data for which $I > 2.58\sigma(I)$. The hafnium atoms were refined anisotropically, and all other non-hydrogen atoms were refined isotropically. Hydrogen atoms on the tmed ligands were included as fixed contributors in idealized positions, and a group isotropic thermal parameter was refined for them. No other hydrogen atoms were included in the refinement. There are two molecules in the asymmetric unit whose metric parameters are generally similar, and each hafnium atom resides on a general position.

(11) NMR studies show that the $^1J_{CH}$ coupling constants are identical in coordinating *and* noncoordinating solvents. We conclude that the Li···C contacts present in the solid-state structure of $[Li(tmed)]_2[Hf(C_2H_4)Et_4]$ are *not* responsible for the unusually small 119-Hz $^1J_{CH}$ coupling constant of the ethylene ligand.

0002-7863/93/1515-2057$04.00/0